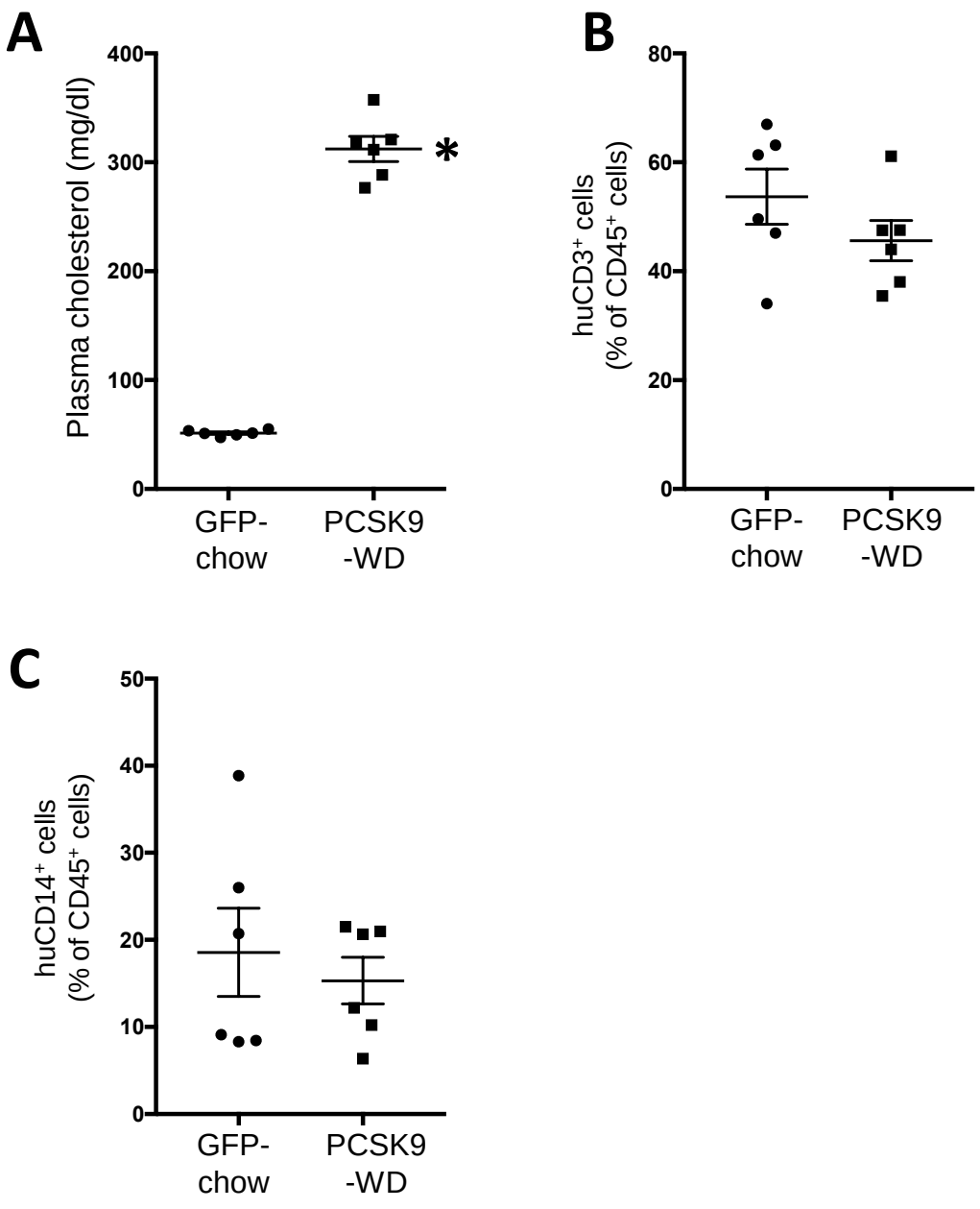

Supplemental Figure 1. Plasma cholesterol is moderately elevated in mice treated with AAV8-TBG-PCSK9 and fed a Western-type diet (PCSK9-WD). Humanized mice were injected with AAV8-TBG-eGFP and chow-fed (GFP-chow) or injected with AAV8-TBG-PCSK9 and fed a WD (PCSKP-WD). **(A)** After 6 weeks (14.5 weeks post-transplant), plasma cholesterol concentration was assayed (n = 6 mice per group; **P* < 0.05, Student's T-test). **(B-C)** Human $CD3^+$ and $CD14^+$ cells in the blood of the indicated groups of mice were assayed by flow cytometry at 10.5 weeks post-AAV injection (19 weeks post-transplant). Data are represented as a proportion of total (mouse + human) $CD45^+$ cells (n = 5-6 mice per group, no statistical differences).

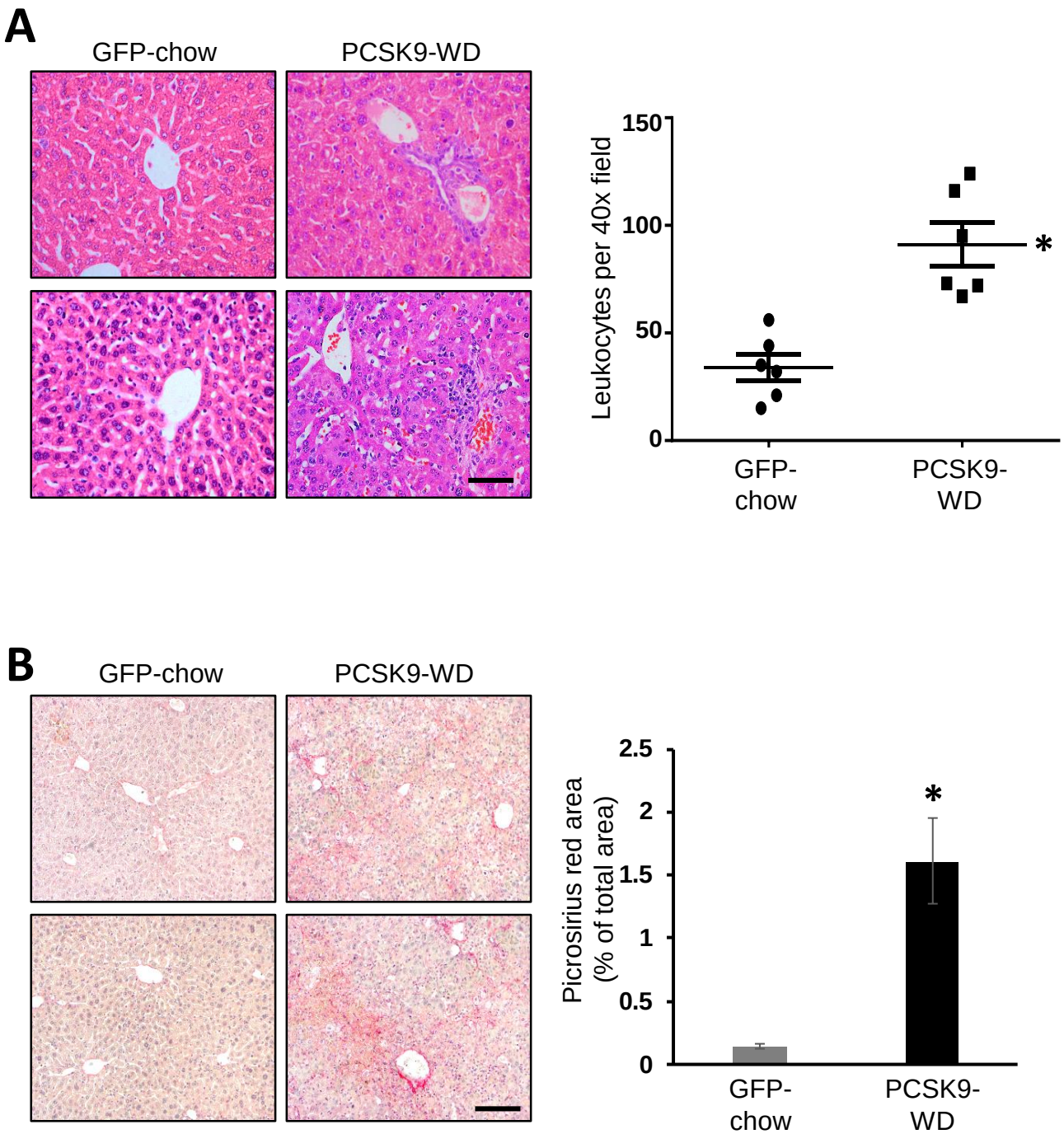

Supplemental Figure 2. Liver inflammation and fibrosis are increased in PCSK9-WD mice from cohort 1. (A) Liver sections were stained with hematoxylin and eosin and leukocytes were counted per 40x field (scale bar, 100 μm). **(B)** Liver sections were stained with picrosirius red to assess fibrosis (scale bar, 200 μm; n = 6 mice per group; *P < 0.05, Student's T-test).

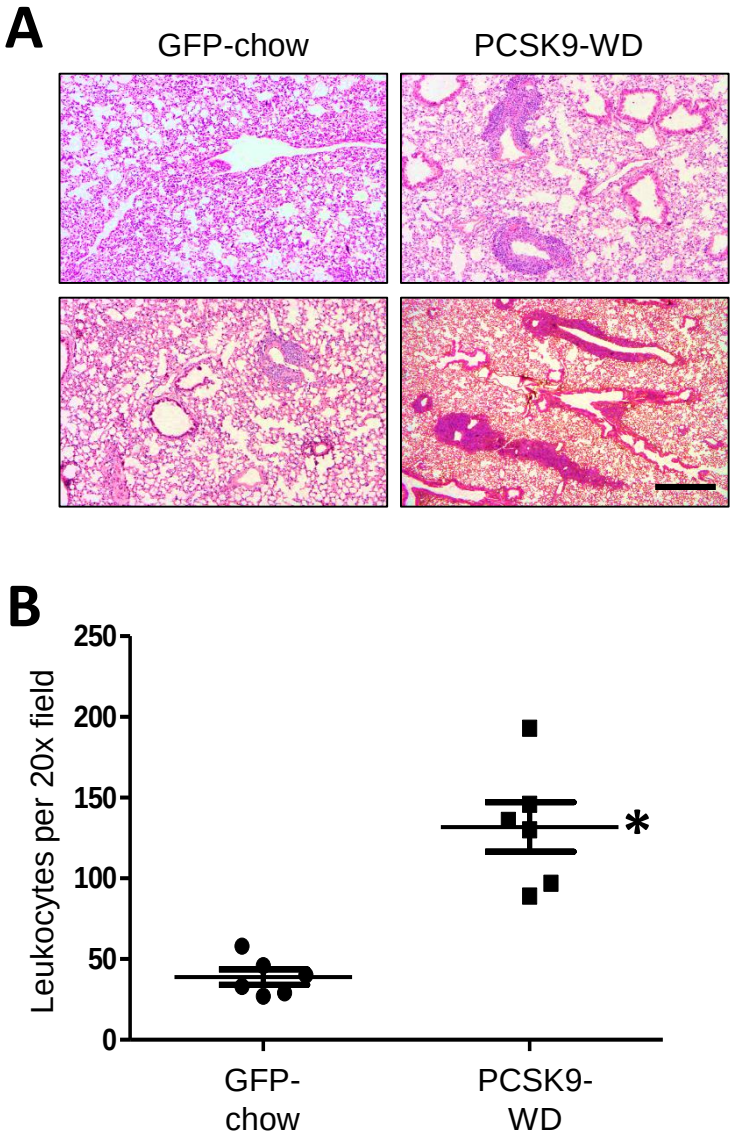

Supplemental Figure 3. Lung inflammation is increased in PCSK9-WD mice from cohort 1. (A) Lung sections were stained with hematoxylin and eosin (scale bar, 500 μm). **(B)** Leukocytes in lung sections were counted and expressed per 20x field (n = 6 mice per group; **P* < 0.05 vs all other groups, Student's T-test).

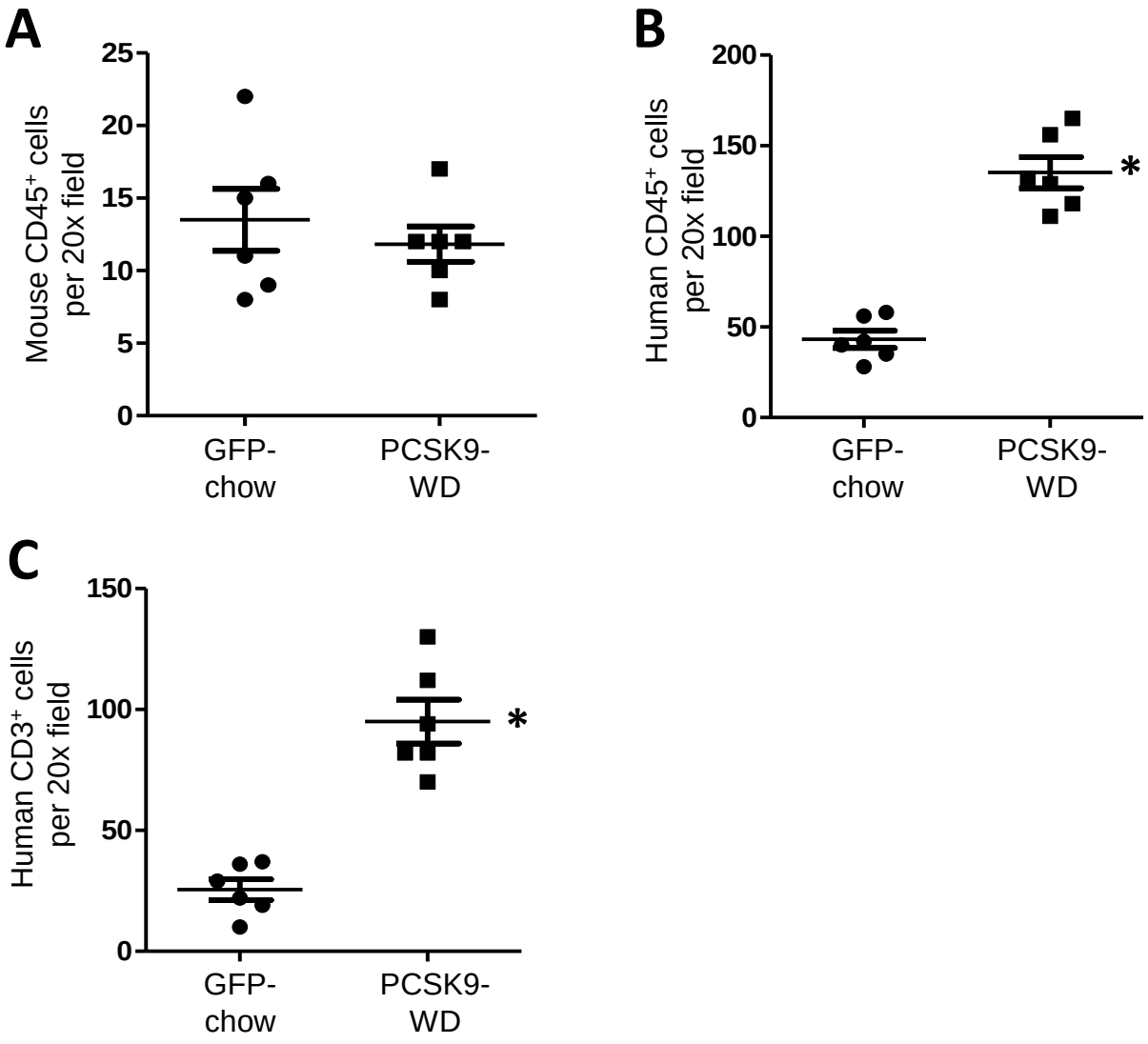

Supplemental Figure 4. Lung leukocytes are primarily human T cells in PCSK9-WD mice from cohort 1. Lung sections were stained and quantified for mouse and human CD45$^+$ cells **(A-B)** and for human CD3$^+$ cells **(C)** (n = 6 mice per group; *P < 0.05, Student's T-test).

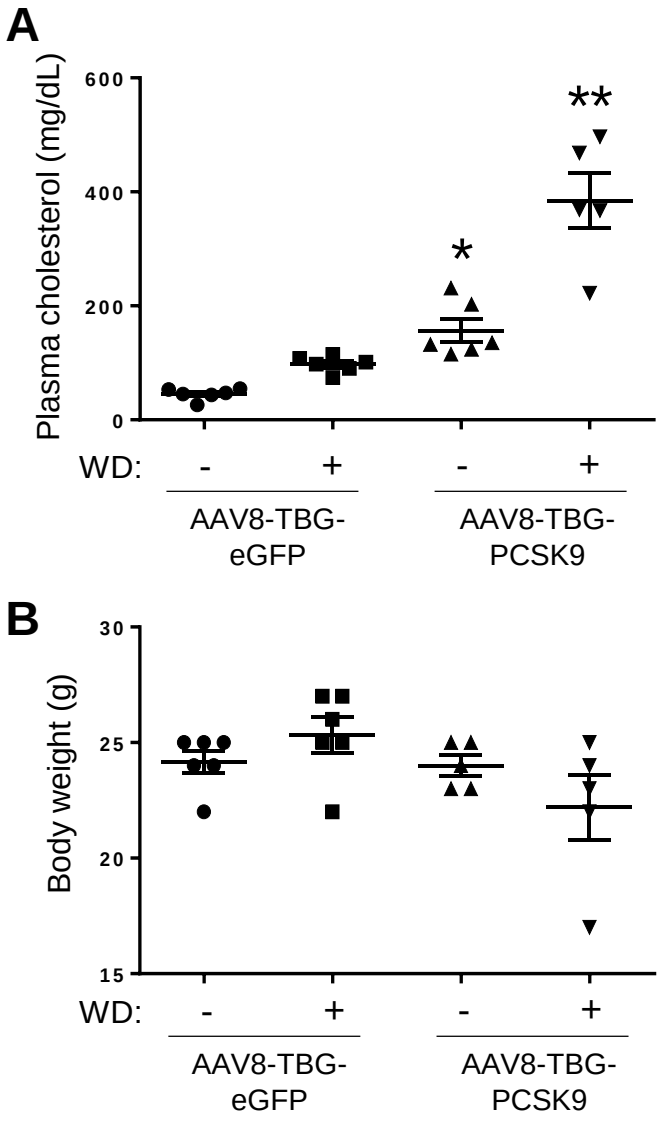

Supplemental Figure 5. Plasma cholesterol and body weight in mice treated with AAV8-TBG-eGFP or AAV8-TBG-PCSK9 and with chow or WD. Thirteen weeks after transplant, mice were injected with AAV8-TBG-eGFP or AAV8-TBG-PCSK9 and placed on a chow or WD. **(A)** After three weeks, plasma cholesterol concentration was assayed (n = 5-6 mice per group; *$P < 0.05$ vs. GFP-chow and PCSK9-WD; **$P < 0.05$ vs all other groups, one-way ANOVA, Tukey's post-hoc analysis). **(B)** Body weight at the time of sacrifice (19 weeks).

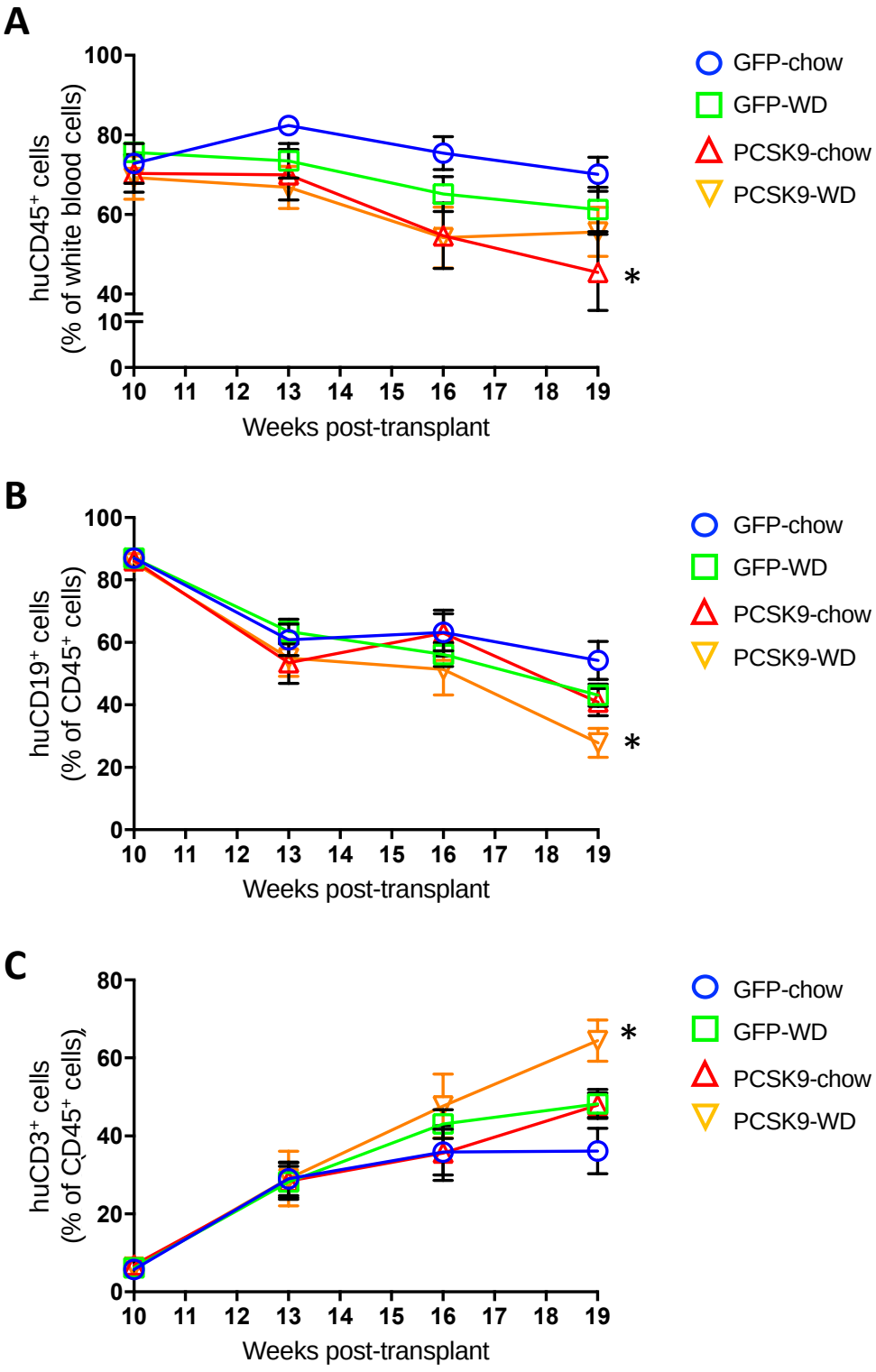

Supplemental Figure 6. Chimerism analysis of circulating white blood cells in hu-mice. Human CD45$^+$ cells, CD19$^+$ cells, and CD3$^+$ cells in the blood of the indicated groups of mice were assayed by flow cytometry at 10, 13, 16, and 19 weeks post-transplant (n = 5-6 mice per group; *P < 0.05 vs. GFP-chow in panel A, two-way ANOVA, Tukey's post-hoc analysis; *P < 0.05 vs. GFP-chow in panel B); and *P < 0.05 vs. GFP-chow in panel C).

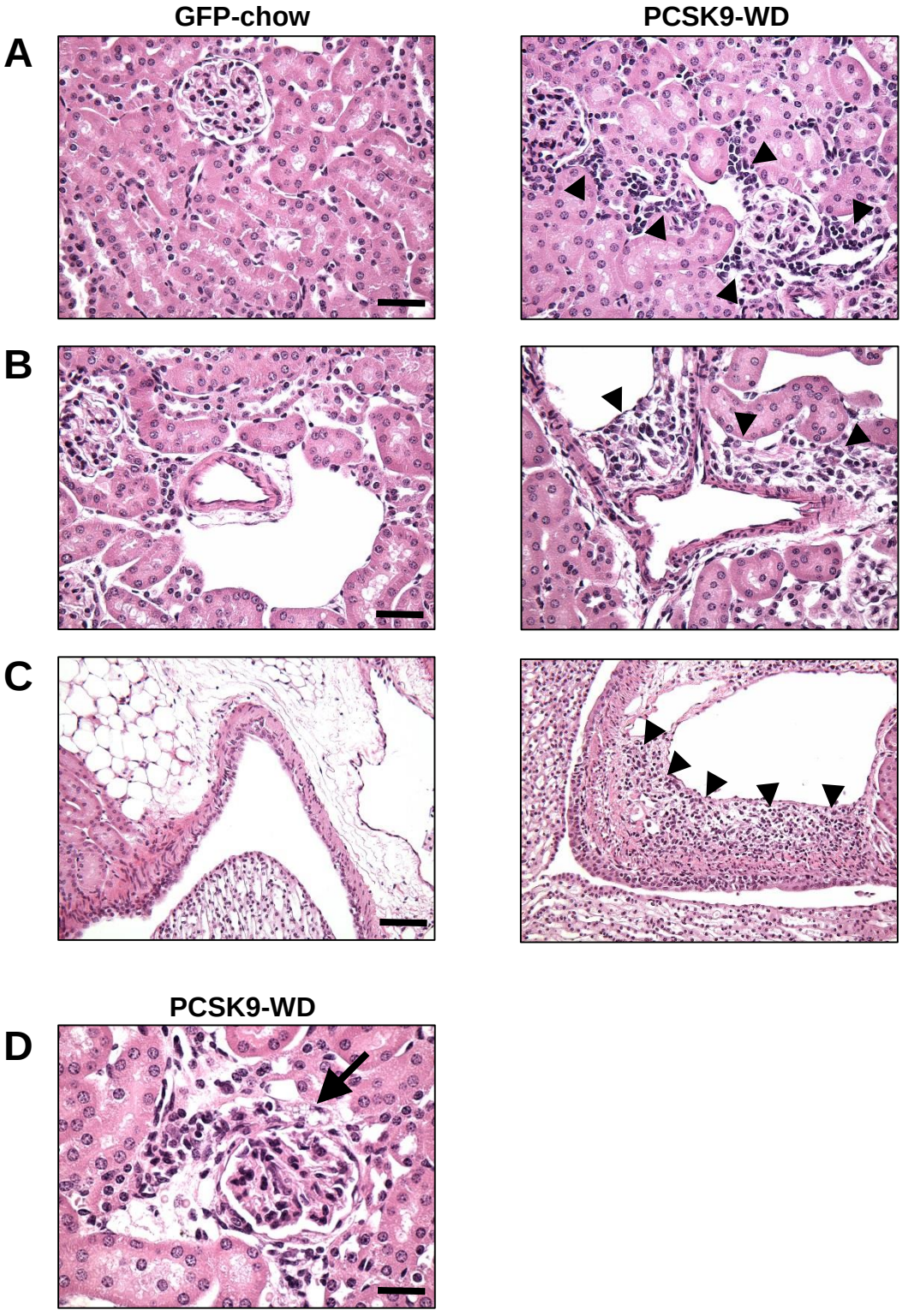

Supplemental Figure 7. Renal inflammation is increased in PCSK9-WD mice. Renal sections were stained with hematoxylin and eosin, and examined by an expert pathologist with findings described as in Supplemental Table 1. (**A**) Illustrative images of interstitial inflammation (400X, scale bar, 50 μm). Arrowheads highlight areas of leukocyte infiltration. **(B**) Illustrative images of perivascular inflammation (400X, scale bar, 50 μm). Arrowheads highlight areas of leukocyte infiltration. (**C**) Illustrative images of peripelvic inflammation (200X, scale bar, 100 μm). Arrowheads highlight areas of leukocyte infiltration. (**D**) Example of interstitial foam cell identified in PCSK9-WD mice shown at arrow (400X, scale bar, 50 μm).

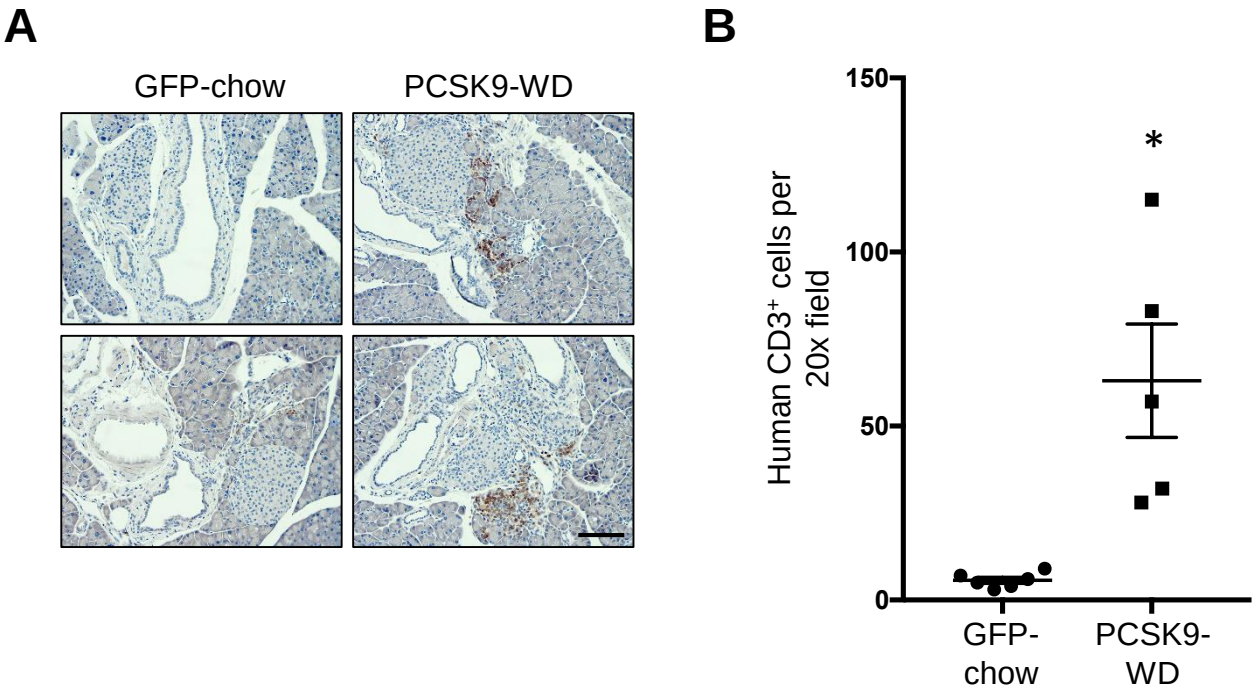

Supplemental Figure 8. Pancreatic inflammation is increased in PCSK9-WD mice. Pancreatic sections were stained with human anti-CD3 antibody. (**A**) Representative images of pancreatic islets at 20X (scale bar, 200 μm). (**B**) CD3 positive cells were counted per 20X field of view (scale bar, 200 μm) (n = 5-6 mice per group; **P* < 0.05 by one way ANOVA with Tukey's post-hoc analysis).

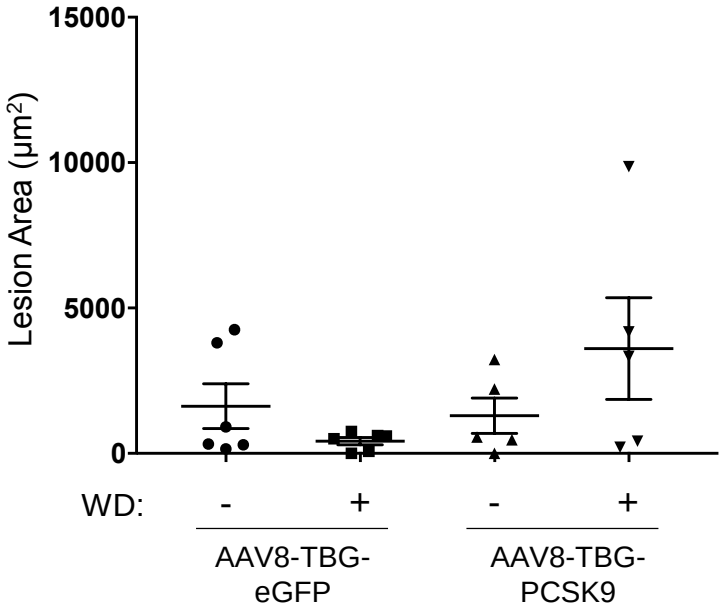

Supplemental Figure 9. Humanized mice do not develop appreciable atherosclerotic lesions. Aortic tissue was harvested from mice 13 weeks post-virus injection and diet feeding (corresponding to 25 weeks post-transplant). Frozen sections of aortic root were obtained and stained with H&E in order to allow assessment of lesion area (n=5-6 per group).

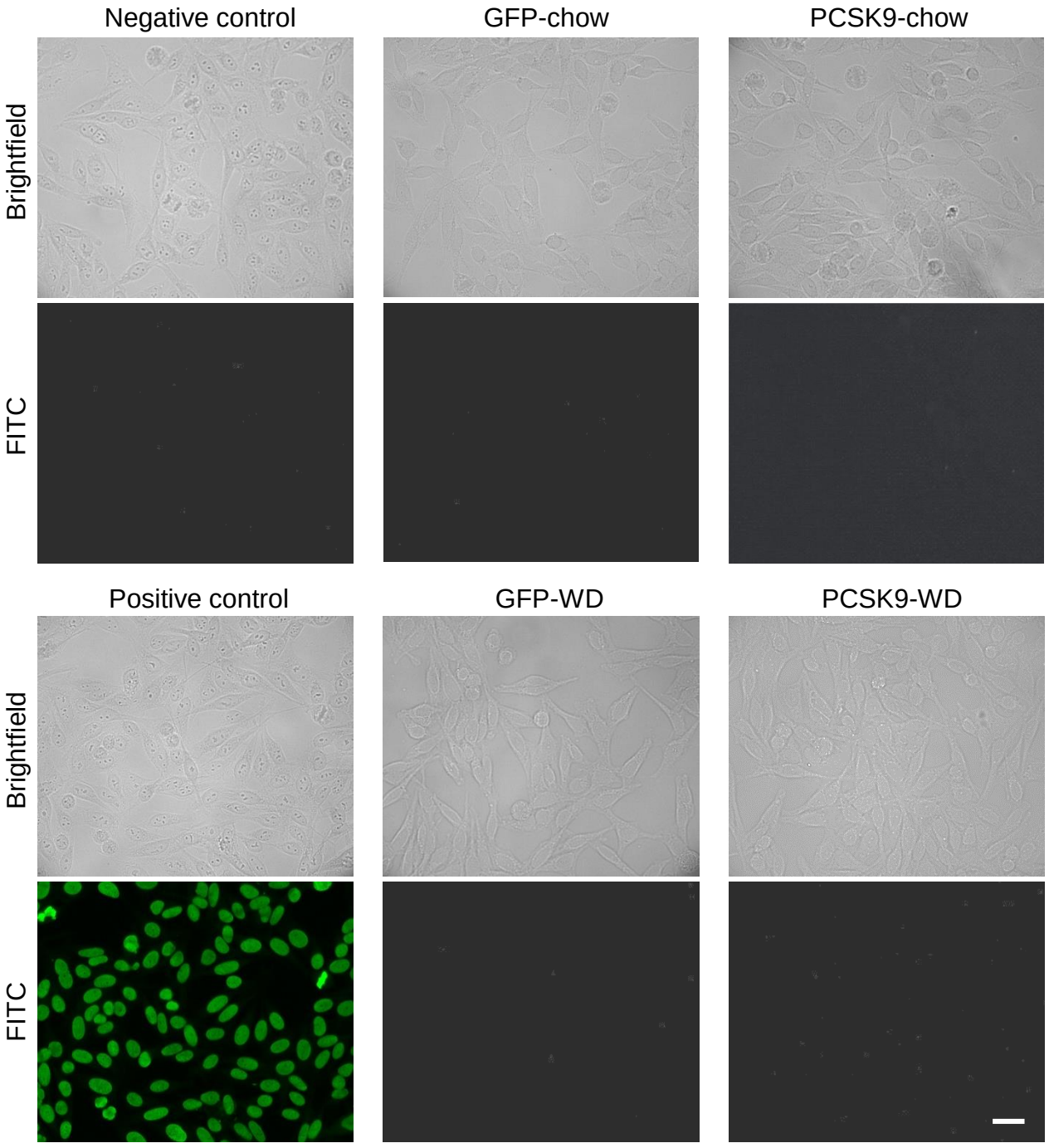

Supplemental Figure 10. Humanized mice do not generate anti-nuclear autoantibodies in response to AAV8-TBG-PCSK9 and/or WD. Human epithelial cell substrate slides were incubated with serum from the cohort of mice in Figure 2 or with positive or negative control serum provided by the manufacturer. An FITC-conjugated secondary antibody was applied to detect bound serum antibody. Representative images are shown; the images incubated with mouse serum were intentionally overexposed to demonstrate true negativity (scale bar, 50 μm; n= 5-6 mice per group). Anti-nuclear antibodies were not detected in any of the plasma samples tested.

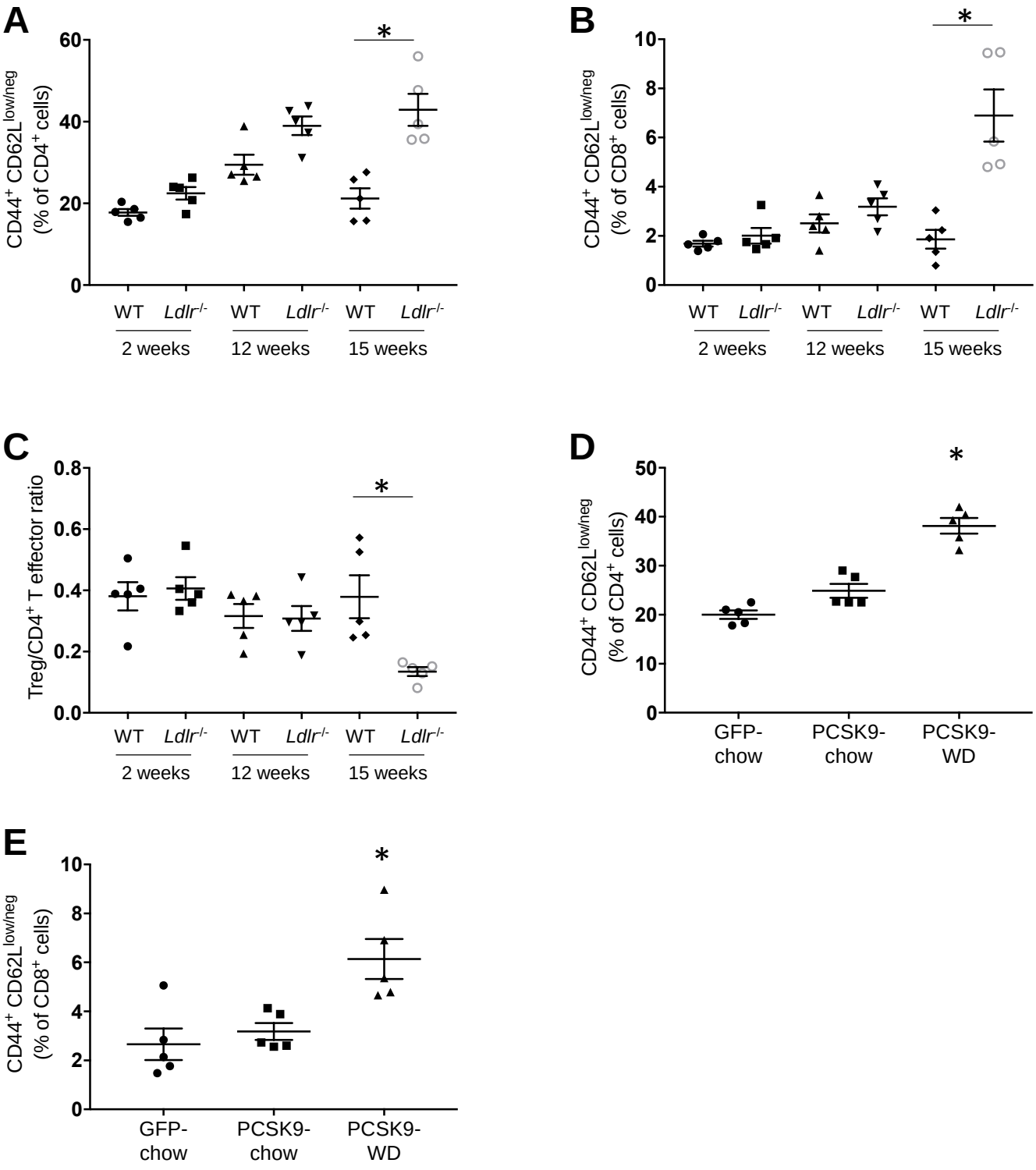

Supplemental Figure 11. T cell subsets in hypercholesterolemic mice. (A-C) The number of $CD4^+$ and $CD8^+$ TEM cells and the ratio of Treg to $CD4^+$ TEM cells were analyzed in the spleens of chow-fed wild-type (WT) mice and WD-fed *Ldlr*$^{-/-}$ mice (n = 5 mice per group; *P < 0.05, one-way ANOVA, Tukey's post-hoc analysis). **(D-E)** WT mice were injected with AAV88-TBG-GFP or AAV88-TBG-PCSK9 and placed on a chow or WD for 10 weeks. Splenic $CD4^+$ and $CD8^+$ T cells were analyzed for an activated phenotype (n = 5 mice per group; *P < 0.05, one-way ANOVA, Tukey's post-hoc analysis).

SUPPLEMENTAL MATERIAL

Proto et al.
Hypercholesterolemia induces T cell expansion in humanized immune mice

Methods

Generation of humanized mice. NOD.scid porcine IL-3-CSF2-KITLG (cohort 1) or NSG (cohort 2) mice were conditioned with sublethal (1.0 Gy) total-body irradiation. Cryopreserved human fetal thymus fragments (1 mm^3) were obtained. At the time of implant, fragments were thawed and agitated prior to insertion in order to minimize pre-existing thymocytes. Fragments were implanted under the kidney capsule followed by intravenous injection with 2 x 10^5 autologous human fetal $CD34^+$ cells within 24 hours of fetal thymus transplantation. All recipients were injected intraperitoneally with anti-human CD2 monoclonal antibody (BTI 322; 400 µg/mouse) on days 0 and 7, again aiming to minimize the transfer of pre-existing thymocytes that may have developed prior to transplant, in the absence of mouse antigens. Human fetal thymus and liver tissues of gestational age 17 to 20 weeks were obtained from Advanced Biosciences Resources. Fetal $CD34^+$ cells were isolated from fetal human liver tissue using a magnetic-activated cell sorter (MACS) separation system with anti-human $CD34^+$ microbeads (Miltenyi Biotec,130-046-703). Two separate cohorts of mice were generated and analyzed, with general reproducibility observed across cohorts.

Viral Transduction. A previously reported rAAV8 encoding a murine gain-of-function (D377Y) PCSK9 was produced by the University of Pennsylvania Vector Core[11]. rAAV8-eGFP was used as a control. Mice were tail vein injected with 10^{12} vg.

Western Diet Feeding. Mice were fed a saturated fat and cholesterol-containing Western diet (WD, Harlan Teklad/Envigo, TD88137) beginning at the time of AAV8-PCSK9 delivery. The first humanized-mouse cohort was fed the diet for approximately 10.5 weeks beginning at 9 weeks post transplantation. The second humanized-mouse cohort was fed diet for 12 weeks beginning at 13 weeks post-transplant. For experiments utilizing WT and *Ldlr*$^{-/-}$ mice, mice were fed the WD *ad libitum* beginning at 10 weeks of age and continuing for up to 15 weeks. Total plasma cholesterol was determined using the Cholesterol E kit (Wako) according to the manufacturer's instructions.

Flow Cytometry of Hu-mice. The level of human hematopoietic cells in peripheral blood mononuclear cells (PBMC), spleen and lung tissues from transplanted mice was screened by flow cytometry and reconstitution was defined as the percent of human CD45 positive cells within the total number of white blood cells. Blood was obtained by submandibular puncture at regular intervals after transplantation to obtain PBMC. Spleens were processed to form a single-cell suspension and then placed through a 40-µm filter. For the isolation of lung infiltrating cells, lung tissues were minced into small pieces and digested with collagenase D (Sigma-Aldrich, COLLD-RO) at 0.5 mg/ml for 45 min at 37°C under agitation conditions followed by filtering digested tissue through a

100 um filter for preparing the single cell suspension. Prior to staining, single cell suspensions were incubated with human AB serum to block nonspecific binding to Fc receptors. Dead cells were excluded from the analysis by gating out low forward scatter and high propidium iodide (PI)–retaining cells. Murine erythroid cells were excluded from the analysis of human chimerism by gating out mouse Ter119+ cells. FCM analysis was performed using a FACSCanto or LSR II (Becton Dickinson), and analysis was carried out by FlowJo software (TreeStar). The following fluorochrome-labelled monoclonal antibodies were used in different combinations for FACS analysis: anti-human CD45 (2D1), CD3 (HIT3a), CD4 (A161A1), CD8 (HIT8a), CD19 (HIB19), CD45RA (HI100), CD45RO (UCHL1), CCR5 (J418F1), CCR7 (G043H7), CD127 (A019D5), CD25 (BC96); anti-mouse CD45 (30-F11) and Ter119; and isotype control antibodies. Anti-human FoxP3 (PCH101) antibodies and Foxp3 staining kit (00-5523-00) were purchased from eBioscience, Thermo Fisher Scientific.

Flow cytometry of WT and Ldlr$^{-/-}$ mice. To analyze splenic T cells, spleens were processed to form a single-cell suspension and then placed through a 40-μm filter. Following red blood cell lysis (Sigma-Aldrich), cells were washed, resuspended in staining buffer consisting of 2% FBS in PBS with 2 mM EDTA, and blocked with anti-mouse CD16/32 antibodies (eBioscience) for 10 minutes. Cells were then incubated with primary antibodies for 30 minutes on ice. Antibodies against CD4 (clone 30-F11), CD8 (clone 53-6.7), CD44 (clone IM7), and CD62L (Clone MEL-14) were purchased from Biolegend. CD25 antibody (clone 7D4) was purchased from eBioscience and CD3 antibody (clone 17A2) was purchased from BD Biosciences. Following surface staining,

cells were incubated with fix/perm buffer (eBioscience), washed with permeabilization buffer (eBioscience), and then incubated with Foxp3 antibody (eBioscience, clone FJK-16s).

Immunofluorescence. Formalin-fixed paraffin embedded tissue sections were deparaffinized using xylene and rehydrated with distilled water. Heat-based antigen retrieval was performed by incubating the sections with citrate-based buffer (Antigen Unmasking Solution, Vector Laboratories, H-3300). The sections were then incubated with protein block solution (Dako, X0909) for 10 minutes to prevent non-specific binding. After 3 washes with 1X PBS, the sections were incubated overnight at 4°C with primary antibodies against human CD45 (Santa Cruz, sc-28369), mouse CD45 (Biolegend, clone 30-F11), or human/mouse CD3 (Abcam, ab16669) diluted in protein block solution. After 3 washes with 1X PBS, the sections were incubated for 1 hour with appropriate fluorophore-conjugated secondary antibody. Images were acquired on a Zeiss fluorescence microscope and analyzed using ImageJ.

Immunohistochemistry. Formalin-fixed paraffin embedded pancreatic sections were deparaffinized using xylene and rehydrated with distilled water. Heat-based antigen retrieval was performed by incubating the sections with citrate-based buffer (Antigen Unmasking Solution, Vector Laboratories, H-3300). The sections were then incubated with protein block solution (Dako, X0909) for 60 minutes to prevent non-specific binding. After 3 washes with 1X PBS, the sections were incubated overnight at 4°C with primary antibodies against human CD3 (Abcam, ab16669) diluted in protein block solution. After

3 washes with 1X PBS, the sections were incubated for 1 hour with HRP-conjugated secondary antibody. After washing in PBS x 3, slides were then developed with DAB (Cell Signaling Technologies) for 10 minutes, then counterstained with hematoxylin and bluing solution. Formalin-fixed paraffin embedded liver sections were processed and stained using an automated clinical Compact Polymer detection system (Bond Polymer Refine Detection, Leica Biosystems) and employing a monoclonal anti-CD3 antibody to detect human T cells (clone LN10, Leica Biosystems).

General histology. Formalin-fixed tissues were paraffin-embedded and then sectioned. Tissue sections were stained with hematoxylin and eosin, according to the manufacturer's protocol (Sigma-Aldrich) and then examined and quantitatively analyzed using a Nikon Labphoto 2 microscope equipped and Image Pro Plus software. Liver inflammation was determined by counting the number of mononuclear cells per field of view (20x, 6 random fields per animal). Liver fibrosis was determined by Picrosirius Red staining (Polysciences, 24901) and the positive area determined with ImageJ software (NIH) (20x, 6 random fields per animal). Lung inflammation scoring was performed according to a previously established method [25]. Briefly, a value of 0 was scored when no leukocytes were detectable, a value of 1 for occasional peribronchial and perivascular cuffing, a value of 2 for consistent cuffing of one to five cells thick, and a value of 3 when cuffing was greater than 5 cells thick. The average of these scores was defined as total lung inflammation (20x, 7 random fields per animal).

Atherosclerotic lesion analysis. At the time of harvest, mice were euthanized using isoflurane. Blood was removed by left ventricular puncture, and the vasculature was then perfused with cold PBS. Aortic roots were placed in OCT and immediately frozen. Serial 8-μm sections were obtained for analysis. For morphometric analysis, six sections 60 μm apart were stained with Harris' H&E. Total lesion and necrotic core areas were defined as previously described (39). All images were captured using a Nikon microscope and analyzed using Image Pro by an observer blinded to the group assignment of each sample.

Assessment of autoantibodies. Plasma samples were obtained from mice at the time of sacrifice and diluted 1:2 prior to analysis. The presence/absence of anti-nuclear antibodies was determined and scored using a NOVA Lite HEp-2 ANA Kit (INOVA Diagnostics, 708100) as per the manufacturer's instructions.

Supplementary Figure Legends

Supplemental Figure 1. Plasma cholesterol is moderately elevated in mice treated with AAV8-TBG-PCSK9 and fed a Western-type diet (PCSK9-WD). Humanized mice were injected with AAV8-TBG-eGFP and chow-fed (GFP-chow) or injected with AAV8-TBG-PCSK9 and fed a WD (PCSKP-WD). **(A)** After 6 weeks (14.5 weeks post-transplant), plasma cholesterol concentration was assayed (n = 6 mice per group; *P < 0.05, Student's T-test). **(B-C)** Human $CD3^+$ and $CD14^+$ cells in the blood of the indicated groups of mice were assayed by flow cytometry at 10.5 weeks post-AAV injection (19 weeks post-transplant). Data are represented as a proportion of total (mouse + human) $CD45^+$ cells (n = 5-6 mice per group, no statistical differences).

Supplemental Figure 2. Liver inflammation and fibrosis are increased in PCSK9-WD mice from cohort 1. (**A**) Liver sections were stained with hematoxylin and eosin and leukocytes were counted per 40x field (scale bar, 100 μm). (**B**) Liver sections were stained with picrosirius red to assess fibrosis (scale bar, 200 μm; n = 6 mice per group; *P < 0.05, Student's T-test).

Supplemental Figure 3. Lung inflammation is increased in PCSK9-WD mice from cohort 1. (**A**) Lung sections were stained with hematoxylin and eosin (scale bar, 500 μm). (**B**) Leukocytes in lung sections were counted and expressed per 20x field (n = 6 mice per group; *P < 0.05 vs all other groups, Student's T-test).

Supplemental Figure 4. Lung leukocytes are primarily human T cells in PCSK9-WD mice from cohort 1. Lung sections were stained and quantified for mouse and human $CD45^+$ cells (**A-B**) and for human $CD3^+$ cells (**C**) (n = 6 mice per group; **P* < 0.05, Student's T-test).

Supplemental Figure 5. Plasma cholesterol and body weight in mice treated with AAV8-TBG-eGFP or AAV8-TBG-PCSK9 and with chow or WD. Thirteen weeks after transplant, mice were injected with AAV8-TBG-eGFP or AAV8-TBG-PCSK9 and placed on a chow or WD. (**A**) After three weeks, plasma cholesterol concentration was assayed (n = 5-6 mice per group; **P* < 0.05 vs. GFP-chow and PCSK9-WD; ***P* < 0.05 vs all other groups, one-way ANOVA, Tukey's post-hoc analysis). (**B**) Body weight at the time of sacrifice (19 weeks).

Supplemental Figure 6. Chimerism analysis of circulating white blood cells in hu-mice. Human $CD45^+$ cells, $CD19^+$ cells, and $CD3^+$ cells in the blood of the indicated groups of mice were assayed by flow cytometry at 10, 13, 16, and 19 weeks post-transplant (n = 5-6 mice per group; **P* < 0.05 vs. GFP-chow in panel A, two-way ANOVA, Tukey's post-hoc analysis; **P* < 0.05 vs. GFP-chow in panel B); and **P* < 0.05 vs. GFP-chow in panel C).

Supplemental Figure 7. Renal inflammation is increased in PCSK9-WD mice. Renal sections were stained with hematoxylin and eosin, and examined by an expert pathologist with findings described as in Supplemental Table 1. (**A**) Illustrative images of

perivascular inflammation (400X, scale bar, 50 μm). Arrowheads highlight areas of leukocyte infiltration. (**B**) Illustrative images of interstitial inflammation (400X, scale bar, 50 μm). Arrowheads highlight areas of leukocyte infiltration. (**C**) Illustrative images of peripelvic inflammation (200X, scale bar, 100 μm). Arrowheads highlight areas of leukocyte infiltration. (**D**) Example of interstitial foam cell identified in PCSK9-WD mice shown at arrow (400X, scale bar, 50 μm).

Supplemental Figure 8. Islet size is increased in PCSK9-WD mice. Pancreatic sections were stained with hematoxylin and eosin, and islet morphology was examined. Measurements of islet area were averaged from a minimum of 10 islets per slide. (**A**) Representative images of pancreatic islets at 20X (scale bar, 200 μm). (**B**) Quantitation of islet area (n=5-6 mice per group, *P<0.05 by one way ANOVA with Tukey's post-hoc analysis). (**C-D**) Pancreatic sections were stained with human anti-CD3 and positive cells were counted per 20X field of view (scale bar, 200 μm) (n = 5-6 mice per group; *P < 0.05 by one way ANOVA with Tukey's post-hoc analysis).

Supplemental Figure 9. Humanized mice do not develop appreciable atherosclerotic lesions. Aortic tissue was harvested from mice 13 weeks post-virus injection and diet feeding (corresponding to 25 weeks post-transplant). Frozen sections of aortic root were obtained and stained with H&E in order to allow assessment of lesion area (n=5-6 per group).

Supplemental Figure 10. Humanized mice do not generate anti-nuclear autoantibodies in response to AAV8-TBG-PCSK9 and/or WD. Human epithelial cell substrate slides were incubated with serum from the cohort of mice in Figure 2 or with positive or negative control serum provided by the manufacturer. An FITC-conjugated secondary antibody was applied to detect bound serum antibody. Representative images are shown; the images incubated with mouse serum were intentionally overexposed to demonstrate true negativity (scale bar, 50 μm; n= 5-6 mice per group). Anti-nuclear antibodies were not detected in any of the plasma samples tested.

Supplemental Figure 11. T cell subsets in hypercholesterolemic mice. (A-C) The number of $CD4^+$ and $CD8^+$ TEM cells and the ratio of Treg to $CD4^+$ TEM cells were analyzed in the spleens of chow-fed wild-type (WT) mice and WD-fed *Ldlr*$^{-/-}$ mice (n = 5 mice per group; **P* < 0.05, one-way ANOVA, Tukey's post-hoc analysis). **(D-E)** WT mice were injected with AAV88-TBG-GFP or AAV88-TBG-PCSK9 and placed on a chow or WD for 10 weeks. Splenic $CD4^+$ and $CD8^+$ T cells were analyzed for an activated phenotype (n = 5 mice per group; **P* < 0.05, one-way ANOVA, Tukey's post-hoc analysis).

Group	Glomerular Retraction	Interstitial Inflammation	Peri-vascular Inflammation	Sub-capsular Inflammation	Peri-pelvic Inflammation	Interstitial Fibrosis	Casts	Comments
GFP/Chow								
1	0	1%	1%	0	0	1%	2	
2	0	0%	0%	0	0	0	0	
3	0	0%	0%	0	0	0	0	
4	0	0%	0%	0	0	0	0	
5	0	0%	0%	0	0	0	0	
6	0	0%	0%	0	0	0	2	
GFP/WD								
1	0	1%	1%	0	0	1%	0	
2	Focal	3%	3%	0	Focal	2%	2	Focal tubular atrophy
3	0	2%	2%	0	0	0	0	
4	0	1%	1%	0	0	0	1	
5	Focal	1%	1%	0	0	1%	0	
6	0	2%	2%	0	0	2%	3	Several interstitial calcifications
PCSK9/Chow								
1	0	2%	2%	0	0	0	2	
2	0	1%	1%	0	0	0	2	Tubular cyst present
3	0	1%	0%	0	0	1%	3	
4	0	1%	1%	0	0	1%	1	
5	Focal	4%	4%	0	0	1%	4	
PCSK9/WD								
1	Focal	3%	3%	0	Focal	2%	0	Rare interstitial foam cells
2	Focal	7%	2%	7%	Focal	7%	0	Subcapsular tubular atrophy
3	0	3%	3%	0	Focal	0	0	
4	0	6%	4%	0	Focal	2%	2	
5	0	4%	2%	0	Focal	2%	0	

Supplemental Table 1. Histological scoring of kidney sections.

Plasma Cholesterol versus:						
% TEM, Compartment	CD4, Blood	CD8, Blood	CD4, Lung	CD8, Lung	CD4, Spleen	CD8, Spleen
R^2	0.2479	0.1723	0.4878	0.3524	0.3813	0.291
p-value	0.0184	0.0548	0.0003	0.0036	0.0029	0.0116

Supplemental Table 2. Correlation of plasma cholesterol with T effector memory populations.